small NANO MICRO

Quantum Dots

A Quantum Dot Photoswitch for DNA Detection, Gene Transfection, and Live-Cell Imaging

*Yuzhou Wu, Klaus Eisele, Mikheil Doroshenko, Gerardo Algara-Siller, Ute Kaiser, Kaloian Koynov, and Tanja Weil**

***Q**uantum dots (QDs) coated with an albumin-derived copolymer shell exhibit significant photoresponsiveness to DNA loading and have great potential for investigating gene delivery processes. The QDs reported herein are positively charged, have attractive optical properties, and are noncytotoxic and notably stable in live cells. Their complex formation with plasmid DNA leads to proportionally decreased photoluminescence and efficient gene transfection is observed. Therefore, they are suitable for live-cell bioimaging and mechanistic studies of nonviral gene delivery. Fluorescence correlation spectroscopy is applied for the first time to investigate individual QDs diffusing in large endosomes inside living cells, and serves as a valuable tool to study the physical properties of QDs inside live cells. The data obtained in this study strongly support the notable stability of these QDs, even in cell endosomes.*

1. Introduction

Quantum dots (QDs) are semiconductor nanoparticles that can serve as powerful fluorescent labels for tracking biological processes in live cells due to their unique properties, such as high photostability, strong photoluminescence, large Stokes shift, and narrow emission spectra.[1] Recently, QDs have been used in gene delivery to elucidate nonviral gene delivery mechanisms.[2–5] Fluorescence resonance energy transfer (FRET) between QDs and organic chromophores has been successfully applied and allows the internalization of nucleic acid/polyelectrolyte complexes and nucleic acid release processes to be followed by independently labeling gene delivery vectors and nucleic acids.[2–5] However, in most cases, the vectors are covalently combined either with nanometer-sized QDs[4] or lipophilic organic dyes,[2,3] which requires additional synthetic steps and may affect the properties of the complexes. Therefore, it would be advantageous to directly investigate QDs as gene delivery vectors. In this context, successful gene silencing has been demonstrated by covalently binding small interfering RNA (siRNA) to amino-functionalized QDs via disulfide linkages[6,7] or by noncovalent adsorption of siRNA onto the surface of positively charged QDs.[8–10] However, in such systems, labeling of nucleic acids is still necessary to investigate siRNA release. Recently, it has also been demonstrated that electron transfer between QDs and DNA induces QD emission quenching,[11,12] which is attractive for the development of label-free DNA detection and delivery systems.

Although using QDs to investigate gene delivery is highly promising, several challenges still obstruct the use of QDs in.vivo. For instance, long-term investigations of QDs in live cells are often limited by the cytotoxicity of QDs at high

Y. Wu, Dr. K. Eisele, Prof. T. Weil
Institute of Organic Chemistry III
Macromolecular Chemistry
Albert-Einstein-Allee 11, 89081 Ulm, Germany
E-mail: Tanja.Weil@uni-ulm.de
M. Doroshenko, Dr. K. Koynov
Max-Planck-Institute for Polymer Research
Ackermannweg 10, 55128 Mainz, Germany
G. Algara-Siller, Prof. U. Kaiser
Electron Microscopy of Materials Science
University of Ulm
89069 Ulm, Germany
G. Algara-Siller
Technical University Ilmenau
98693 Ilmenau, Germany

DOI: 10.1002/smll.201200409

© 2012 Wiley-VCH Verlag GmbH & Co. KGaA, Weinheim

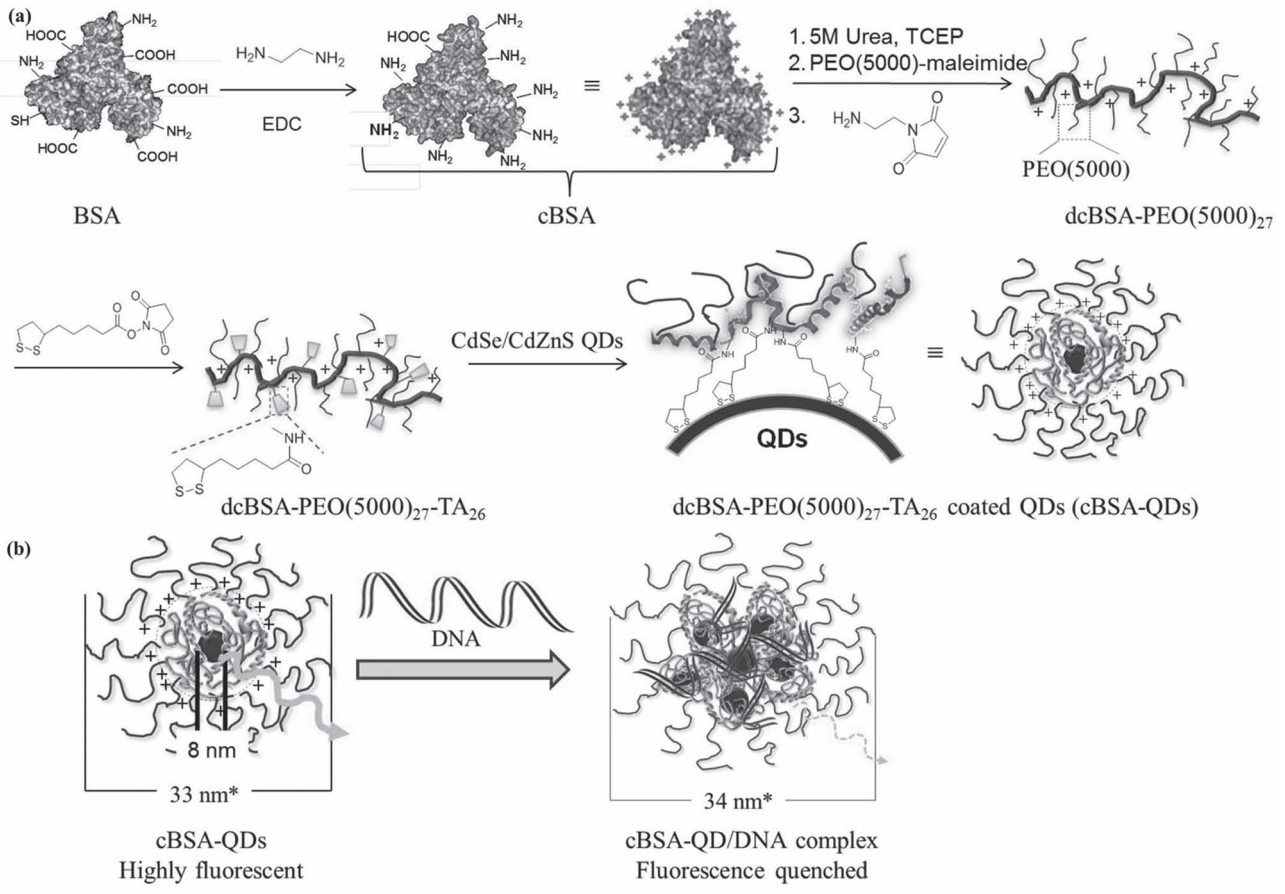

Scheme 1. Illustration of a) cBSA-QDs preparation and b) cBSA-QD/DNA complex formation. *Hydrodynamic diameter according to dynamic light scattering. EDC=*N*-ethyl-*N*′-[3-(dimethylamino)propyl]carbodiimide hydrochloride, TCEP=(2-carboxyethyl)phosphine.

concentrations, and long-term stability studies of QDs in a biological environment have not been conclusive.[1,13] Therefore, it is still of great interest to develop noncytotoxic QDs with high in vivo stability, which offer the unique possibility to investigate efficient gene delivery and release in live cells.

Herein, we present the encapsulation of QDs using a tailored grafted polycationic polyethylene oxide (PEO)–polypeptide copolymer that results in a remarkably stable coating on the QDs via multivalent interactions (**Scheme 1**). Such grafted cationic polypeptides are derived from cationized bovine serum albumin (cBSA-147), which possesses particularly low cytotoxicity and has been used previously as a vehicle to efficiently transfer DNA into cells, thereby allowing stable gene transfection.[14] Previously, serum albumins as abundant proteins have been applied as QD coatings. Notable advantages of BSA as a surface coating have been demonstrated, including good solubility in salted buffer and under physiological conditions, ready availability and inexpensiveness, and biocompatibility, as well as the presence of a large variety of free functional groups.[15,16] Recently, we have reported the preparation of pH-responsive QDs after coating with a human serum albumin (HSA)-derived copolymer with grafted PEO chains via ligand exchange (HSA-QDs).[17] HSA-QDs with negative net charges are attractively biocompatible, but they are not taken up by cells due to the charge repulsion between the HSA-QDs and the cell membrane. Herein, we report the preparation of a novel polypeptide copolymer, dcBSA-PEO$(5000)_{27}$-TA_{26}, derived from denatured and cationized bovine serum albumin (dcBSA)[14] with about 27 grafted PEO(5000) chains and about 26 thioctic acid (TA) groups distributed along the polypeptide backbone. This polymer was applied to coat QDs (cBSA-QDs), which reveal unique properties ideally suited for live-cell imaging, such as efficient cellular uptake, high intracellular stability, and low cytotoxicity. Complex formation of cBSA-QDs with plasmid DNA reveals a significant photoresponsive behavior. Therefore, these QDs provide an attractive platform for investigating DNA transport and DNA unpacking during gene delivery. In addition, it is often time-consuming to identify the optimal ratio of the transfection reagent and DNA. Here, due to the photoresponsive behavior of cBSA-QDs, optimal cBSA-QDs to plasmid DNA ratios for efficient gene transfection can be conveniently assessed from the emission intensities of the cBSA-QD/DNA complexes. We applied fluorescence correlation spectroscopy (FCS) to study the sizes, aggregation behavior, and stability of single QDs in live cells. Individual, freely diffusing cBSA-QDs were observed inside large endosomes and, to the best of our knowledge, similar studies collecting the physical properties of QDs inside live cells have not yet been reported. Therefore, cBSA-QDs are

 © 2012 Wiley-VCH Verlag GmbH & Co. KGaA, Weinheim

attractive for live-cell imaging, and these results pave the way toward mechanistic studies of nonviral gene delivery processes.

2. Results and Discussion

2.1. Preparation of cBSA-QDs

The grafted cationic polypeptide copolymer (dcBSA-PEO$(5000)_{27}$-TA_{26}) was synthesized by a similar procedure to that reported previously for an HSA-derived anionic copolymer,[17] which is briefly depicted in Scheme 1. BSA was first cationized by reacting most of the carboxylic acid groups of the glutamate and aspartate residues with ethylenediamine.[14,18] Thereafter, cationized BSA (cBSA-147)[14] was denatured in the presence of urea, and tris(2-carboxyethyl)phosphine (TCEP) was applied to reduce all 17 disulfide bridges, thereby yielding 34 additional thiol groups. In situ reaction of approximately 27 PEO(5000)-maleimide chains with the accessible thiol groups and capping of unreacted thiol groups with aminoethyl maleimide gave dcBSA-PEO$(5000)_{27}$. The subsequent attachment of approximately 26 TA moieties[17] to lysine residues yielded the final copolymer, dcBSA-PEO$(5000)_{27}$-TA_{26}. The interaction of dcBSA-PEO$(5000)_{27}$-TA_{26} with hydrophobic as-synthesized CdSe/CdZnS QDs (quantum yield (QY) 48%) was achieved after reduction of the disulfide groups of the TA substituents with $NaBH_4$ under an argon atmosphere and subsequent addition of QDs dispersed in a minimum amount of THF. The ligand exchange reaction was carried out overnight, and the resulting QDs modified with dcBSA-PEO$(5000)_{27}$-TA_{26} were then isolated after filtration through a 0.2-μm syringe filter. After coating, QDs covered with dcBSA-PEO$(5000)_{27}$-TA_{26} (cBSA-QDs) were homogeneously dispersed in water, and the emission spectra revealed a small bathochromic shift relative to the as-synthesized QDs in hexane (Figure S2, Supporting Information), consistent with previous reports on ligand exchange with thioalkyl acids.[19] cBSA-QDs with a QY of 21% at pH 7 were obtained via this approach.

2.2. Characterization of cBSA-QDs

2.2.1. Size Determination of cBSA-QDs

The CdSe/CdZnS cores were visualized by transmission electron microscopy (TEM) as homogeneously dispersed particles with average diameters of about 8 nm (**Figure 1**b; for large TEM images, see Figure S3, Supporting Information). Since the protein shell of cBSA-QDs could not be visualized by TEM directly, dynamic light scattering (DLS, Figure 1c) and FCS (**Figure 2**d) were applied to assess the hydrodynamic diameter of cBSA-QDs. Hydrodynamic diameters of cBSA-QDs of 33 and 44 nm, respectively, were obtained from DLS (polydispersity index (PDI) of 0.19, Figure 1c) and FCS analysis, the latter with a good fitting to a one-component correlation. The significantly larger hydrodynamic diameter relative to the CdSe/CdZnS core reflects the successful coating by the cBSA-copolymer shell. Therefore, to contribute to the average diameter of cBSA-QDs in solution, both DLS and FCS data were considered resulting in an average hydrodynamic diameter of about 38.5 nm. This value correlates very well to the theoretical estimation of 39 nm for cBSA-QDs (for detailed calculation, see Supporting Information section 6). The diameters obtained by applying different methods are summarized in **Table 1**.

2.2.2. cBSA-QDs Exhibit High Stabilities

The high number of TA groups attached along the copolymer backbone allows multivalent interactions to stabilize the QDs in solution, thus yielding extremely stable core–shell particles even under extreme conditions.[20] No changes in the optical spectra occurred even after 6 months of storage at 4 °C. High stability was also found in phosphate-buffered saline (PBS) and cell culture medium (Dulbecco's modified Eagle's medium (DMEM); Figure 1f). Furthermore, although the biopolymer dcBSA-PEO$(5000)_{27}$-TA_{26} undergoes fast enzymatic degradation in solution, the QDs coated with dcBSA-PEO$(5000)_{27}$-TA_{26} exhibited very high resistance to proteolysis. The incubation of cBSA-QDs with trypsin (0.1 mg mL^{-1}) and proteinase K for 2 h resulted in only a slight decrease in the QY (Figure 1f and Figure S6, Supporting Information), which suggests strong interactions of multiple thiol groups with the QD surface. In addition, the presence of a PEO shell should reduce the accessibility of epitopes, minimize plasma protein binding, and enhance metabolic stability.[21] All of these results strongly suggest that cBSA-QDs are highly attractive for live-cell imaging experiments.

2.2.3. Polycationic cBSA-QDs Facilitate Fast Cell Uptake

Charges play an important role in cellular uptake, cell trafficking, and targeting of subcellular structures[22,23] and the presence of positive or negative charges will determine the location and function of QDs in.vivo. Therefore, coating the surface of QDs allows fine-tuning of their surface properties such as surface charges and functionalities, which are crucial factors for cell imaging experiments. The plasma protein HSA has an isoelectric point of 4.9, whereas cBSA-147 displays an isoelectric point of 9.5. Gel electrophoresis at pH 7.4 (Figure 1d) shows that HSA-modified QDs move toward the positive electrode and cBSA-147-modified QDs toward the negative electrode, thus demonstrating net negative and net positive charges of HSA-QDs[17] and cBSA-QDs, respectively.

The cellular uptake efficiency into A549 cells (an adenocarcinoma human alveolar basal epithelial cell line) was studied with both cBSA-QDs and HSA-QDs,[17] and in the case of polyanionic HSA-QDs,[17] no significant cellular uptake was observed after 24 h of incubation, most likely due to electrostatic repulsion between the negatively charged QDs and the cell membranes (Figure S7a, Supporting Information). In contrast, polycationic cBSA-QDs revealed significant cellular uptake and enrichment in the perinuclear region (Figure S7b, Supporting Information). A similar uptake behavior has also been observed for the precursor protein cBSA-147,[14] an efficient gene transfection reagent that crosses cell membranes via clathrin-mediated endocytosis and localizes in the

© 2012 Wiley-VCH Verlag GmbH & Co. KGaA, Weinheim

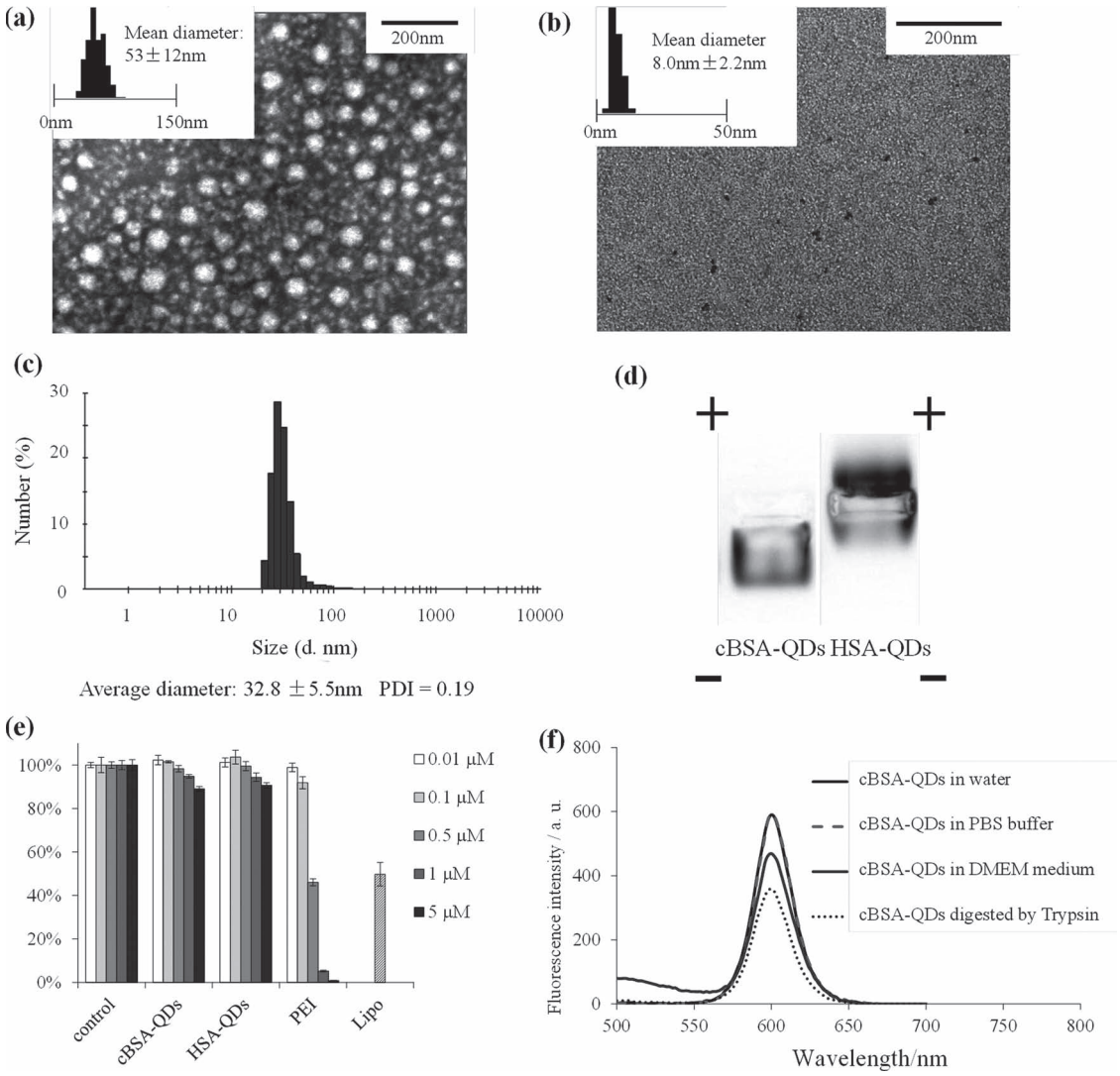

Figure 1. Preparation and characterization of cBSA-QDs. a) TEM image of cBSA-QDs stained with uranyl acetate. The inset shows the size distribution based on a statistic of 133 particles (mean ±standard deviation (SDV)). b) Direct TEM image of cBSA-QDs displaying QD cores. The inset reveals the size distribution based on a statistic of 106 particles (mean ± SDV). c) Hydrodynamic diameter distribution measured by DLS (mean ±SDV). d) Fluorescence image of gel electrophoresis with cBSA-QDs performed at pH 7.4. cBSA-QDs with a positive net charge move toward the negative electrode (anode) and HSA-QDs[17] with a negative net charge move toward the positive electrode (cathode). e) Cytotoxicity of cBSA-QDs and negatively charged HSA-QDs[17] in A549 cells after a 24 h of incubation. PEI and Lipo were included for comparison. Lipo was tested using the manufacturer's recommended concentration for 450 ng plasmid DNA transfection (bar with crossed paths). Data were obtained in triplicate, and standard deviations are shown as error bars. f) Study of the stability of cBSA-QDs in water, PBS, and DMEM and after trypsin digestion. The same concentrations of cBSA-QDs were incubated in various media for 24 h, and the emission spectra were recorded (λ_{ex} = 254 nm).

endoplasmic reticulum (ER) and Golgi apparatus.[14] The cell uptake mechanism of cBSA-QDs has been investigated by applying filipin, which blocks caveolae-mediated endocytosis, and chlorpromazine, which inhibits clathrin-mediated endocytosis. We observed that treatment with chlorpromazine reduced the cBSA-QDs uptake (p<0.005) while application of filipin did not affect cell uptake (p>0.1) according to confocal microscopy (Figure S12, Supporting Information), thus indicating clathrin-mediated endocytosis as one of the major pathways. The opportunity to manipulate the cellular uptake of QDs is of great importance for a wide range of applications: high cellular uptake via clathrin-mediated endocytosis and release from vesicles allows investigation of intracellular targets, whereas low-level cellular uptake facilitates imaging of extracellular structures, such as the extracellular matrix or cell surface receptors.

2.2.4. cBSA-QDs Are Not Cytotoxic

Cytotoxicity assays were further performed using the CellTiter-Glo cytotoxicity assay kit and no significant cell toxicity was observed for cBSA-QDs at concentrations up to 5 μM after 24 h of incubation with A549 cells (Figure 1e). In comparison, the polycationic gene delivery agent polyethylenimine (PEI) revealed significant cell toxicity at similar concentrations (Figure 1e). In addition, Lipofectamine 2000 (Lipo), one of the most commonly used transfection

 © 2012 Wiley-VCH Verlag GmbH & Co. KGaA, Weinheim

small NANO MICRO

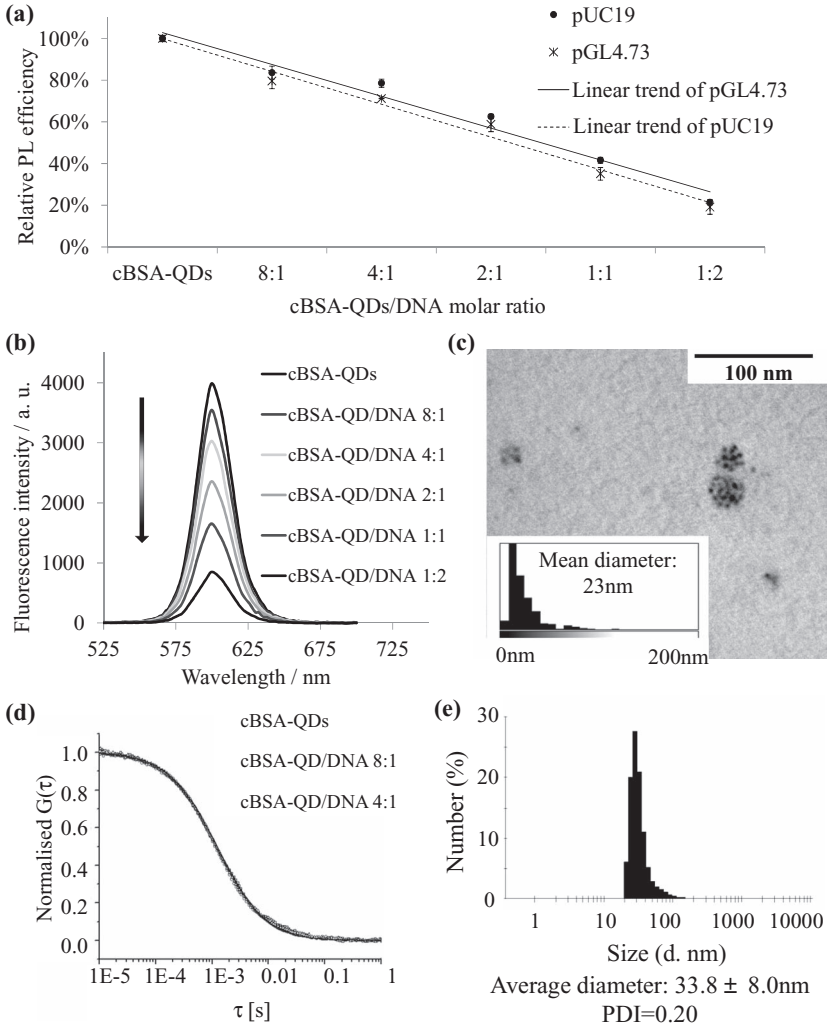

Figure 2. Characterization of cBSA-QD/DNA complexes and gene transfection. a) Relative PL efficiency of complexes with different ratios (cBSA-QD/DNA). pUC19 and pGL4.73 were tested as representative plasmid DNA. Data were obtained in triplicate, and standard deviations are shown as error bars. b) Emission spectra of different complex ratios (cBSA-QD/pUC19-DNA); $\lambda_{ex} = 254$ nm. c) TEM images of 8:1 cBSA-QD/DNA complexes (see TEM images of complexes formed by other polyelectrolyte ratios and large-area images in Figure S4, SupportingInformation). d) FCS autocorrelation curves measured for cBSA-QDs and pUC19 plasmid complexes in aqueous solution at approximately 10 nM concentration. The solid lines represent the corresponding best-fit lines with single-component equations. e) Hydrodynamic diameter distribution measured by DLS. The average diameter was calculated based on three independent measurements and the standard deviation is presented as error.

reagents, also displayed significantly higher cytotoxicity at relevant concentrations (Figure 1e). Low cytotoxicity of the chemically modified protein precursor cBSA-147[14] has been reported before and was attributed to the noncytotoxic nature of the protein-based polymer coating, which effectively protects the QD core through multivalent interactions. Due to the low cytotoxicity, higher concentrations of cBSA-QDs can be applied to cell experiments as compared to QDs coated with synthetic polymers that are usually applied at nanomolar concentrations.[6]

2.3. cBSA-QD/DNA Complexes Exhibit Remarkable Photoresponsiveness

Surface charges are among the key factors affecting the interaction between QDs and guest molecules and polycationic nanoparticles are known to undergo strong interactions with nucleic acids.[4,8,24] It has been shown previously that cBSA-147 efficiently complexes plasmid DNA and high transfection efficiencies were found.[14] Interestingly, in vitro experiments on the complex formation of cBSA-QDs with different proportions of two kinds of plasmid DNA of varying lengths (pUC19, 2686 base pairs (bp), and pGL4.73, 3921 bp) revealed significant changes in the optical properties of the QDs. Increasing the ratio of DNA to cBSA-QDs from 1:8 to 2:1 resulted in a continuous reduction of the photoluminescence (PL) efficiency to less than 20% of the original PL (Figure 2a). It is unlikely that the observed significant quenching of the PL was caused by aggregate formation, which usually causes spectral broadening or spectral shifts, since neither changes in the emission spectra nor shifts in the emission maxima of the QDs were observed (Figure 2b) in the presence of DNA.[25,26] Probably, electron transfer between QDs and nucleotide bases plays a major role, supported by the fact that DNA-induced quenching was recently reported for cysteine-capped QDs,[11] which was attributed to electron transfer between QDs and nucleotide bases.[11,12] However, the exact mechanism of quenching

Table 1. Summary of size and optical properties of cBSA-QDs and cBSA-QD/DNA complexes (8:1).

Sample	Relative PL efficiency [%][b)]	Diameter [nm] (TEM)[c)]	Hydrodyn. diameter [nm](DLS)	Hydrodyn. diameter [nm](FCS)	Theor. hydrodyn. diameter [nm][d)]
cBSA-QDs	100 ± 2[e)]	8 ± 2[e)]	33 ± 6[e)]	≈44	39
cBSA-QD/DNA complexes (8:1)[a)]	84 ± 3[e)]	23 ± 16[e)]	34 ± 8[e)]	≈44	

[a)]pUC19 plasmid was used as DNA; [b)]Relative PL efficiency was calculated by considering the PL efficiency of cBSA-QDs as 100%; [c)]The statistical diameter of QD core clusters measured according to direct TEM images; [d)]For detailed calculation, see Supporting Information; [e)]Average ± SDV.

© 2012 Wiley-VCH Verlag GmbH & Co. KGaA, Weinheim

is still elusive. It is a particular feature that the emission of the cBSA-QDs was not quenched entirely, most likely due to the cBSA polymer backbone serving as a distance holder between the cBSA-QDs and the DNA nucleobases. Residual emission of the complexes is crucial for investigating both the complexes and free QDs via fluorescence microscopy, as discussed below in more detail. Efficient formation of stable cBSA-QD/DNA complexes was further supported by gel electrophoresis (Figure S8, Supporting Information), in which no free DNA or cBSA-copolymer was detected in the cBSA-QD/DNA complexes.

The morphologies of the complexes formed by different cBSA-QDs to DNA ratios were investigated by TEM (Figure 2c and Figure S4, Supporting Information) and FCS (Figure 2d). In TEM measurements, cBSA-QDs were visualized as individual 7 nm QD cores (Figure 1b), whereas cBSA-QD/DNA complexes (Figure 2c) were observed as condensed aggregates with average diameters of 23 nm. Varying the cBSA-QD/DNA ratio from 8:1 to 1:1 did not significantly influence complex morphologies or sizes (Figure S4, Supporting Information). cBSA-QD/DNA 8:1 complexes studied by FCS and DLS experiments revealed slightly larger hydrodynamic diameters of 44 and 34 nm, respectively, in the same range as those of individual cBSA-QDs in solution (Figure 2 d,e and Table 1). Most likely, complex formation with DNA condenses the extended, soft, and flexible copolymer shell consisting of soft PEO chains, thereby yielding nanosized cBSA-QD/DNA complexes with hydrodynamic radii similar to those of individual cBSA-QDs but with a more dense and compact structure.

In addition, the changes of the emission intensities of cBSA-QDs upon complex formation with DNA were studied with FCS (Figure 2d) by measuring the average particle brightness (see Experimental Section), which is directly proportional to the QY of the studied fluorescent species. A particle brightness of cBSA-QDs of 24 kHz per particle for free cBSA-QDs, 21 kHz per particle for 8:1 cBSA-QD/DNA complexes, and 19 kHz per particle for 4:1 cBSA-QD/DNA complexes was found, which suggests an easily detectable photoresponsiveness with a similar trend to that observed in the emission spectra. The remarkable photoresponsiveness of cBSA-QDs represents an efficient indicator of DNA complex formation, which could be very attractive for DNA detection and the convenient monitoring of DNA loading and unpacking in live cells without the need to apply other labels or DNA modifications.

2.4. cBSA-QD/DNA Complexes Efficiently Transfect Mammalian Cells

The potential of cBSA-QDs to efficiently deliver plasmid DNA into cells was evaluated by transfecting pGL4.73 plasmid DNA, which encodes for the Renilla luciferase. cBSA-QD/DNA complexes formed with different QD-to-DNA ratios were tested (**Figure 3** and Figure S13, Supporting Information) and successful expression of luciferase was investigated by applying the Renilla-Glo Luciferase Assay System (Promega, Mannheim) based on luminescence

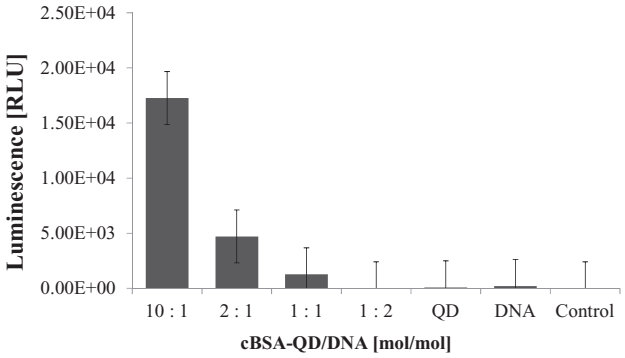

Figure 3. Gene transfection efficiencies of cBSA-QDs measured using the Renilla-Glo Luciferase Assay. Data were obtained in triplicate, and standard deviations are shown as error bars. Experiments were repeated three times independently.

detection. Successful gene transfection was achieved but the transfection efficiencies were strongly dependent on the applied cBSA-QD/DNA ratio (Figure 3). It is well known that optimal positive-to-negative charge ratios of the polyelectrolytes are required to accomplish efficient gene transfection, since cellular uptake of the complexes, DNA protection, and DNA release are important factors in this process that need to be fine-tuned experimentally.[14] Interestingly, complexes formed with high cBSA-QD content that were strongly fluorescent also revealed increased transfection efficiencies, whereas increased DNA content in the complexes that also displayed low fluorescence intensities yielded strongly reduced transfection efficiencies. Low transfection efficiencies in the presence of high DNA quantities could indicate inefficient cellular uptake of the complexes and/or inefficient DNA protection from proteolysis. cBSA-QD/DNA complexes formed in a 10:1 ratio possess an adequate net positive charge to facilitate efficient cellular uptake and DNA release (higher ratios of cBSA-QDs and DNA were not tested since quenching of the emission intensities could not be detected anymore, which renders such complexes less useful). Usually, the positive-to-negative charge ratios of polyelectrolyte complexes must be calculated and carefully adjusted experimentally, which is often challenging and time-consuming, particularly for less well defined transfection and transduction facilitators. Here, due to the photoresponsive behavior of cBSA-QDs, optimal cBSA-QDs to plasmid DNA ratios for efficient gene delivery could be conveniently assessed from the emission intensities of the complexes.

2.5. Confocal Imaging and FCS Studies Allow Investigation of cBSA-QDs and cBSA-QD/DNA Complexes in Live Cells

In the next step, the cellular uptake and vesicle trafficking of cBSA-QDs and cBSA-QD/DNA complexes were investigated using confocal imaging and FCS. FCS represents a powerful technique that can be used to study the dynamic behavior of fluorescent species (small molecules, macromolecules or nanoparticles) in various environments. The method is based on monitoring and recording the fluctuations of the

 © 2012 Wiley-VCH Verlag GmbH & Co. KGaA, Weinheim

NANO MICRO small

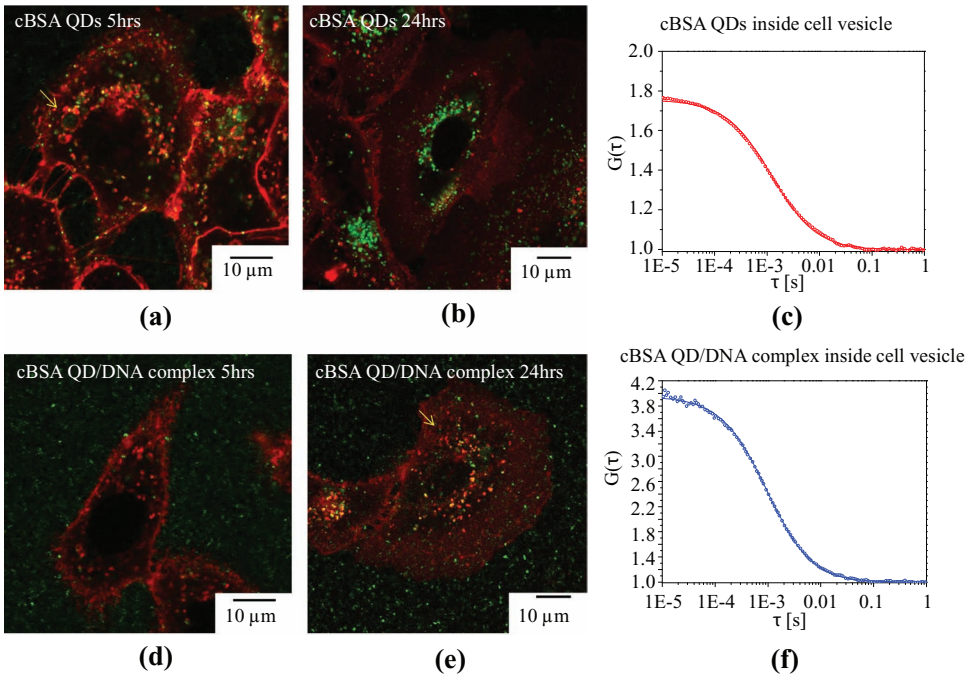

Figure 4. Confocal imaging of cBSA-QDs and 8:1 cBSA-QD/DNA complexes. a) cBSA-QDs incubated with A549 cells for 5 h.b) cBSA-QDs incubated with A549 cells for 24 h. c) Representative FCS autocorrelation curves of QDs measured in live cells treated with cBSA-QDs after 5 h.d) cBSA-QD/DNA complexes (8:1) incubated with A549 cells for 5 h. e) cBSA-QD/DNA complexes (8:1) incubated with A549 cells for 24 h.f) Representative FCS autocorrelation curves of QDs measured in live cells treated with cBSA-QD/DNA complexes (8:1) after 24 h. Cell membranes were labeled with CellMaskDeepRed tracker and are shown in red in the photomicrographs, and cBSA-QDs (recorded using 488 nm excitation and 555–605 nm bandpass emission filter) are shown as green points. Arrows show the position where the FCS focus was located to measure QD properties in live cells.

fluorescence intensity signal, caused by the diffusion of the species through a very small, stationary observation volume (typically the focus of a confocal microscope) positioned at the point of interest in the studied sample. The recorded fluctuations were evaluated in the form of an autocorrelation curve that was then fitted with appropriate model equations (see Experimental Section) to obtain quantitative information on the physical properties of the species. One of the most common applications of FCS includes measuring the hydrodynamic radii of diffusing fluorescent species: from the autocorrelation curve, the mean residence time of the species in the focal observation volume can be determined. Knowing the size of the observation volume and the diffusion coefficient, through the Stokes–Einstein relation the hydrodynamic radius of the fluorescent species as well as the number of fluorescent species in the observation volume (i.e., the local concentration) and their particle brightness can be assessed. The latter parameter is determined by dividing the average fluorescence intensity by the number of species in the observation volume and is a measure of the fluorescence brightness of an individual specimen. Due to minimal requirements on sample amounts and its high sensitivity and selectivity, FCS has found widespread applications, for example, for probing quantities such as diffusion coefficients, kinetic rate constants, and equilibrium binding constants.[27] Owing to the very small observation volume of FCS (<1 μm^3), such studies can be performed inside living cells or even in subcellular compartments.[28,29] Therefore, FCS represents a valuable technique to elucidate the behavior of cBSA-QDs in live cells. To the best of our knowledge, live-cell imaging with QDs has not been investigated by FCS before.

A549 cells were treated with cBSA-QDs (≈0.2 µM), and the intracellular pathway was followed by time-lapse confocal microscopy and FCS. CellMask Deep Red tracker was used to label the cell and intracellular membranes. cBSA-QDs were found to accumulate on the cell surface within 2 h (Figure S9a, Supporting Information), thus indicating that an adsorptive endocytosis process occurs in which the first step is the electrostatic accumulation of the highly cationic QDs on the negatively charged cellular membrane.[30] Subsequently, the bound QDs were internalized into early endosomes when the cellular membrane invaginated to form endocytotic vesicles. Once inside the cells, cBSA-QDs remained in vesicles at different locations in the cells, as confirmed by FCS studies performed after 5 h of incubation. These studies, performed by positioning the observation volume on different places in the cells, showed no freely diffusing QDs in the cells, and only occasionally were large and bright objects detected. These large objects most likely represented endosome vesicles slowly passing through the observation volume.

Furthermore, the confocal microscopy images revealed the presence of several large and immobile endosome lumens. By positioning the FCS observation volume (<1 μm^3) inside such lumens (arrow in **Figure 4**a), we were able to study the properties of endosome-entrapped QDs. Interestingly, monodispersed QDs and no aggregates were observed (Figure 4c).

© 2012 Wiley-VCH Verlag GmbH & Co. KGaA, Weinheim

Assuming that the viscosity in the endosome is equal to that of water, the hydrodynamic radii of these QDs were in the range of approximately 24 nm, which is slightly smaller than in aqueous solution. This could be due to partial enzymatic degradation of the accessible, unbound parts of the biopolymer shell, which has also been observed in vitro (Figure S6, Supporting Information). However, the presence of high ion concentrations and the influence of the differing viscosities in vesicles and water on diffusion times may also have an impact on the calculated sized of the cBSA-QDs. QDs with a reduced brightness of approximately 9 kHz per particle were recorded inside the vesicles. However, due to the different excitation setup for this cell study and the complicated membrane environment in the cells, the brightness of each QD could not be directly compared with that obtained in solution. The ability to investigate coated QDs inside late endosomes strongly supports the excellent stability of the cBSA-QDs, even under high salt and more acidic conditions as well as in the presence of enzymes in live cells. Aggregate formation of QDs inside cells and the association of QDs with cell membranes are normally considered important limitations for QD applications in.vivo.[1,13] Thus, cBSA-QDs exhibit highly promising live-cell imaging features, most likely due to the multivalent interactions stabilizing the protein coating and to the presence of polyethylene glycol (PEG) chains, which minimize the nonspecific adsorption of QDs.

After 24 h of incubation, cBSA-QDs were found accumulated at a specific pole of the cell perinuclear region, the region where the ER and Golgi apparatus are located (Figure 4b), and displayed a very similar trafficking behavior to the gene transfection vehicle cBSA-147.[14] This accumulation was further confirmed by staining cell ER with ER-Tracker Green dye, which showed co-localization of QD signals within the ER region (Figure S10, Supporting Information). In addition, in some endosomal vesicles, freely diffusing cBSA-QDs could still be detected with similar size distributions and emission intensities to those in previous investigations (Figure S11, Supporting Information).

Thereafter, cBSA-QD/DNA (8:1) complexes, which represent a good compromise of sufficient transfection efficiencies and detectable changes of the emission intensities, were investigated in A549 cells. Slower uptake was observed compared with cBSA-QDs due to the presence of fewer net positive charges (Figure 4 d,e). Large endosomes containing freely diffusing cBSA-QD/DNA that can be studied by FCS were only found after the 24 h incubation time. This observation emphasizes the delicate interplay between the number of positive charges and cellular uptake efficiency, which has been previously highlighted for polymers and for cationic lipid carrier systems.[31–33] The FCS measurements showed the presence of nonaggregated and rather monodispersed QD-based objects in the endosomes. Interestingly, these objects had size distributions (diameter = 24 nm) and particle brightnesses (8 kHz per particle; Figure 4f) similar to those measured for the cBSA-QDs in endosomes without complexation with DNA (Figure 4c), thus indicating that the cBSA-QDs may have already released their cargo DNA. Since live cells represent highly complex and dynamic systems, additional studies

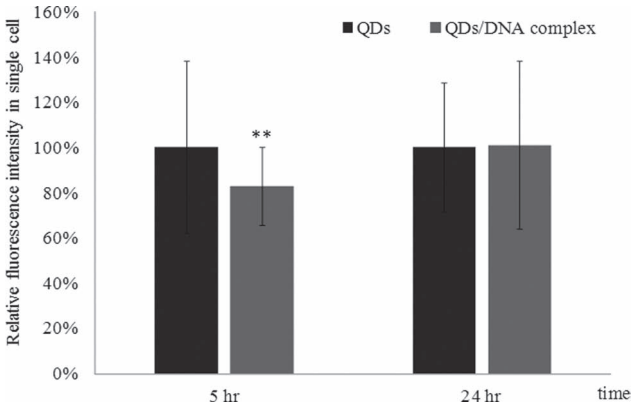

Figure 5. Statistical quantification of the emission intensities of QDs in individual cells based on 25 to 30 cells. Asignificantly lower emission intensity (20% less) was observed after investigating cells treated with cBSA-QD/DNA complexes (8:1) compared to cBSA-QDs after 5 h. After 24 h, similar emission intensities were regained for both samples by investigating the same cells. $**p<0.005$ by ANOVA test.

are required to achieve an improved understanding of the sophisticated interplay of aggregation, disaggregation, and membrane association in these vesicles. The co-localization of 8:1 cBSA-QD/DNA complexes with endosomes and the accumulation within the ER region were also observed by membrane staining and ER-Tracker Green dye staining (Figure S10, Supporting Information), thereby indicating that the internalization process of 8:1 cBSA-QD/DNA complexes proceeds similar to that for cBSA-QDs.

In addition to FCS quantification, a statistical quantification on the total brightness of cBSA-QDs and cBSA-QD/DNA complexes in individual cells was performed at two different time points during the transfection process by applying confocal microscopy. We treated A549 cells in two different experiments with the same amount of a) cBSA-QDs and b) cBSA-QD/DNA complexes for 5 h and confocal images using the same settings (e.g., excitation laser power and detector gain) were acquired. After 5 h, all QDs that were not taken up by the cells were removed by multiple washing steps in both experiments and the cells were further cultured in fresh medium. Confocal images of these cells were taken after 5 h and again after 24 h with identical microscope settings. The emission intensities of the QDs of experiments (a) and (b) in each single cell were quantified using ImageJ software based on a statistics of about 25 to 30 cells. As shown in **Figure 5** (for representative cell images, see Supporting Information Figure S9), cBSA-QD/DNA complexes in experiment (b) exhibited a significantly lower (≈20% less) emission intensity ($p < 0.005$ by the analysis of variance (ANOVA) test) compared to cells treated with cBSA-QDs in experiment (a) after 5 h, whereas the identical emission intensities were regained after 24 h. These experimental data are in good agreement with the partially quenched fluorescence intensity of cBSA-QD/DNA complexes at the beginning of the gene transfection experiment (about 20% quenching for 8:1 complexes calculated for 100% emission intensity of cBSA-QDs) and recovery of the emission intensity after DNA release after 24 h. Although

© 2012 Wiley-VCH Verlag GmbH & Co. KGaA, Weinheim

comprehensive studies are still needed to elucidate the entire process of DNA release from cBSA-QDs, results from both FCS and confocal imaging strongly suggest the release of DNA cargoes and recovery of cBSA-QDs after 24 h, which is well in line with the gene transfection experiments.

3. Conclusion

In summary, we have prepared a noncytotoxic, protein-derived biopolymer coating for efficiently encapsulating QDs, and have demonstrated that these coated QDs are highly photoresponsive in the presence of DNA and facilitate efficient cellular uptake, gene delivery, and particle analysis in living cells by FCS.

cBSA-QDs bear several positive charges to facilitate interactions with negatively charged cell membranes and to enable efficient cellular uptake via clathrin-mediated endocytosis. Due to the protein-type nature of the coating, cBSA-QDs exhibit very low cytotoxicity, even at high concentrations and high stability in different buffers and inside the cell vesicles, such as in the late endosomes. These unique features are likely to be due to the multivalent interactions between the dcBSA-PEO$(5000)_{27}$-TA_{26} copolymer and the QD surface and to the presence of multiple PEO chains. In addition, cBSA-QDs electrostatically interact with DNA to form stable polyelectrolyte complexes. Upon complex formation with DNA, significant photoresponsiveness was detected, as measured by a decrease in the emission intensity with increasing DNA content. Quenching was attributed to electron transfer between DNA and cBSA-QDs and not to aggregate formation due to the absence of spectral changes. Optimal complex ratios for gene transfection were characterized by high cBSA-QD content (e.g., cBSA-QD/DNA ratios of 8:1 or 10:1) and high emission intensities of the QDs in the complexes. Such complexes formed with equimolar quantities or with DNA in excess exhibited low emission intensities due to DNA-induced quenching, and they only displayed low transfection efficiencies most likely due to low cellular uptake or low DNA condensation/protection in the complexes. In this way, DNA concentrations required for efficient gene delivery could be conveniently assessed from the emission spectra of the QDs.

For the first time, FCS was successfully applied to investigate cBSA-QDs in intracellular endosomes, and confirmed again that cBSA-QDs are very stable inside living cells. Charging DNA onto cBSA-QDs led to the observed decreased QD PL efficiencies. These cBSA-QD/DNA complexes have great potential to evolve as a valuable tool to follow DNA packing and release without the necessity to directly label the DNA. Preliminary studies using live-cell FCS reveal recovery of PL efficiency after DNA release.

We envision that cBSA-QDs, with all of their unique features, could be explored as valuable photoresponsive and noncytotoxic markers attractive for in vivo bioimaging to acquire an improved mechanistic understanding of nonviral gene delivery. Furthermore, the presence of several available functional groups along the protein backbone provides various opportunities for introducing additional modifications on QDs, such as signaling peptides.

4. Experimental Section

Materials: All chemical reagents were obtained from commercial suppliers and used without further purification unless otherwise noted. Bovine serum albumin (BSA), *O*-(2-maleimidoethyl)-*O′*-methyl-polyethylene glycol 5000 (PEO(5000)-MI; >90% purity by NMR spectroscopy), and branched polyethylenimine (PEI; 25 kDa) were purchased from Sigma–Aldrich. cBSA-147 was synthesized according to our previous report.[14] Succinimide-activated thioctic acid (TA-NHS) was prepared according to a previously reported procedure.[34] Bio-Rad Bio-Gel P30 was used for desalting. Vivaspin ultrafiltration tubes were purchased from GE Healthcare. Dulbecco's modified Eagle's medium (DMEM; 1X, high glucose), fetal bovine serum (FBS) standard quality (EU approved), and penicillin/streptomycin solution (100X) were purchased from PAA Laboratories GmbH, Germany. MEM (nonessential amino acid solution 10 mM (100X)), LysoTracker Green DND-26, ER-Tracker Green dye, CellMask Deep Red plasma membrane stain, Lipofectamine 2000 transfection reagent (Lipo), and Leibovitz's L-15 Medium (1X), containing L-glutamine but no phenol red, were purchased from Invitrogen. The CellTiter-Glo Luminescent Cell Viability Assay kit and the Renilla-Glo Luciferase Assay System were obtained from Promega GmbH, Germany. CdSe/CdZnS QDs were synthesized according to previously reported procedures[35] and kindly provided by Dr. Yinthai Chan (National University of Singapore, Singapore).

Instruments: The fluorescence and absorbance were recorded using a Tecan M-1000 microplate reader. ÄKTA Purifier FPLC and Sephacryl S-100 HR gel filtration columns were used for dcBSA-PEO$(5000)_{27}$ purification. Vivaspin 20 (molecular weight cutoff (MWCO) 30 000) and Vivaspin 6 (MWCO 10 000) devices obtained from GE Healthcare were used for ultrafiltration, and the centrifugation was performed using an Eppendorf 5804R centrifuge at 3500 rpm. Precast NuPAGE TA 3–8% Gel and NuPAGE Bis–Tris 4–12% Gel were purchased from Invitrogen, and gel electrophoresis was performed in an Invitrogen Novek Mini-Cell. The confocal microscopy and FCS measurements were performed using a FV300 laser scanning confocal system (Olympus, Japan) coupled to an inverted optical microscope IX-70 (Olympus, Japan).

Preparation of dcBSA-PEO$(5000)_{27}$-TA_{26}-Coated QDs (cBSA-QDs): dcBSA-PEO$(5000)_{27}$-TA_{26} was prepared following a reported procedure (see Supporting Information for details).[17] To prepare cBSA-QDs, dcBSA-PEO$(5000)_{27}$-TA_{26} (1 mg, ≈6.6 nmol) was dissolved in pure water (2 mL). Then, $NaBH_4$ (1 mg, 26 μmol) was added under argon, and the reaction mixture was stirred for 2 h to reduce all disulfide bridges of the TA groups. After reduction, HCl (1 M) was added until no more gas formed. Subsequently, NaOH (1 M) was added to adjust the solution to a neutral pH. CdSe/CdZnS QDs (5 equiv, 33 nmol) in THF (10 μL) were added to the reduced dcBSA-PEO500027-TA26 under vigorous stirring. After sonication for 1 min, the reaction mixture was constantly stirred overnight. Thereafter, the reaction mixture was filtered through a 0.2 μm microsyringe filter to eliminate any uncoated QDs that precipitated from aqueous solution. Finally, the water-soluble cBSA-QDs were further purified and concentrated by ultrafiltration (Vivaspin 6 MWCO 10 000).

© 2012 Wiley-VCH Verlag GmbH & Co. KGaA, Weinheim

Measurement of Relative PL Efficiency of cBSA-QDs Complexed with Different DNAs: The concentration of cBSA-QDs was firstly estimated by determining dcBSA-PEO$(5000)_{27}$-TA_{26} copolymer concentration using the BCA (bicinchoninic acid) protein assay kit (Pierce). Desired molar ratios of different plasmid DNAs were then added to the same amount of cBSA-QDs solutions and the complex solutions (20 μL) were transferred to a 384-well small-volume black microplate (Grenier Bio-one). The emission spectra of the QDs and QD/DNA complexes were first checked, and no shift in the spectrum was found. The maximum emission intensity at 600 nm (λ_{ex} = 254 nm) was recorded for each sample. The relative PL efficiency was calculated by dividing the emission intensity of each sample by the emission intensity of the original QDs at the same concentration.

Cell Culture: A549 cells, a human alveolar basal epithelial carcinoma cell line, were obtained from DSMZ (German Collection of Microorganisms and Cell Cultures, Braunschweig). Cells were cultured in high-glucose DMEM supplemented with 10% FBS, penicillin (100 U mL^{-1}), streptomycin (0.1 mg mL^{-1}), and nonessential amino acids (0.1 mM) at 37 °C in a humidified 5% CO_2 incubator.

Luciferase Gene Transfection Assay: A549 cells were seeded at a density of 8000 cells per well in a white 96-well plate and were incubated overnight at 37 °C in 5% CO_2. Subsequently, cBSA-QD/DNA complexes were prepared at different ratios. All complexes were suspended in a final volume of 50 μL with Tris-HCl (100 mM) and NaCl (100 mM), pH 7.2, and were incubated for 5 min. Cells were washed twice gently with prewarmed PBS. Then, warm PBS (50 μL) containing 2% glucose and each complex (50 μL) containing pGL4.73 plasmid (450 ng) in Tris-HCl buffer were added to the corresponding wells and incubated for 45 min to allow maximum interaction with the cell membrane. Subsequently, A549 cells were supplied with fresh supplemented DMEM (100 μL) without antibiotics and then incubated overnight at 37 °C in 5% CO_2 to enable sufficient transfection and gene expression. The transfection efficiency was quantified using the Luciferase Assay System (Promega, Mannheim) according to the manufacturer's protocol with a delay time of 2 s and a detection time of 15 s.

Cytotoxicity Assay: A549 cells (8000 cells per well) were plated onto a white 96-well plate and incubated overnight to allow attachment. The wells were 70–80% confluent on the day of the experiment. The cells were treated with cBSA-QDs, HSA-QDs, PEI, or Lipo at relevant concentrations and incubated for an additional 24 h. Blank cells without treatment were used to obtain 100% cell viability. After treatment, the Cell-Titer Glo (Promega) cell viability assay kit was used to quantify the viability of the cells in each well according to the manufacturer's instructions.

Confocal Microscopy Imaging: A549 cells were plated in a Coverglass Lab-Tek eight-well chamber (Nunc, Denmark) at a density of 30 000 cells per well in DMEM (300 μL) containing 10% FBS, 1% penicillin/streptomycin, and 1% MEM. The cells were incubated overnight at 37 °C in 5% CO_2 to allow adhesion. The next day, the cells were washed gently twice with prewarmed PBS and then incubated in warm PBS (100 μL) containing 2% glucose in cBSA-QDs solution (32 μL, 1 μM; sterilized with a 0.2 μm microsyringe filter) or the cBSA-QD/DNA complex (8:1 cBSA-QDs/pUC19 plasmid; 1 μM) for 2 h. Subsequently, L-15 medium (100 μL) without phenol red and supplemented with 10% FBS and 0.1 mM nonessential amino acids was supplied to cells, which were further incubated for the desired time at 37 °C under 5% CO_2. Imaging was then performed using a FV300 laser scanning confocal system (Olympus, Japan) coupled to an inverted optical microscope IX-70 (Olympus, Japan) equipped with a 60×/1.2 NA water immersion objective (Olympus, Japan). The QD fluorescence was excited with the 488 nm line of an argon laser, and fluorescence was detected after a 555–605 nm bandpass emission filter. The membrane dye was excited with a He–Ne laser at 633 nm, and the fluorescence was collected after an LP650 long-pass emission filter. During the experiments, the samples were mounted on a temperature-controlled microscope stage (Linkam, UK), which kept the cells at 37 °C.

FCS in Solution and Inside Live Cells: Fluorescence correlation spectroscopy (FCS) was carried out using the FV300-IX-70 system (Olympus, Japan). For the FCS studies, the fluorescence signal after passing through the confocal pinhole of FV300 was fiber guided to a single-photon counting avalanche photodiode detector connected to a TimeHarp 200 time-correlated single-photon counting card (both PicoQuant, Germany). The data acquisition and analysis were completed using the SymPhoTime software package (PicoQuant, Germany). For the FCS studies in live cells, cells were treated the same as for confocal imaging. An image was firstly acquired using the FV300-IX-70 system, and then the focus of the microscope was positioned at a point of interest using the galvanometric scanning mirrors of the FV300 instrument and its Fluoview software package. The focus was kept there during the FCS data acquisition. The measured autocorrelation curves were fitted with the model function given in Equation (1) to determine the hydrodynamic radii of the diffusing species:

$$G(\tau) = 1 + \frac{1}{N}\left(1 + \frac{\tau}{\tau_D}\right)^{-1}\left(1 + \frac{\tau}{S^2\tau_D}\right)^{-1/2} \quad (1)$$

where N is the average number of fluorescent species in the observation volume V, τ_D is the lateral diffusion time, and $S = z_0/\omega_0$ is the ratio of the axial to the radial dimensions of V. The diffusion coefficient of the fluorescent species D can be calculated by $D = \omega^2_0/4\tau_D$, and the hydrodynamic radius can be calculated using $R_H = k_BT/6\pi\eta D$, where T is the temperature, k_B the Boltzmann constant, and η the viscosity of the solution. Furthermore, the average fluorescent particle brightness, which is directly proportional to the QY of the studied fluorescent species, was evaluated by dividing the average fluorescence intensity (in kHz) by the average number of fluorescent species N in the observation volume. The calibration of the size of the observation volume V was performed using a tracer with a known diffusion coefficient, Alexa Fluor 488.

Supporting Information

Supporting Information is available from the Wiley Online Library or from the author.

Acknowledgements

The authors acknowledge Andreas Best from the Max-Planck-Institute for Polymer Research for his assistance with the FCS and Y. T. Chan and Y. Xu from the National University of Singapore for

 © 2012 Wiley-VCH Verlag GmbH & Co. KGaA, Weinheim

kindly providing the CdSe/CdZnS QDs. We also acknowledge the financial support from the DFG within the Sonderforschungsbereich SFB 625 and under grant P3246 029 DFG.

[1] X. Michalet, F. F. Pinaud, L. A. Bentolila, J. M. Tsay, S. Doose, J. J. Li, G. Sundaresan, A. M. Wu, S. S. Gambhir, S. Weiss, *Science* **2005**, *307*, 538.
[2] H. H. Chen, Y. P. Ho, X. Jiang, H. Q. Mao, T. H. Wang, K. W. Leong, *Mol. Ther.* **2008**, *16*, 324.
[3] Y. P. Ho, H. H. Chen, K. W. Leong, T. H. Wang, *J. Control. Release* **2006**, *116*, 83.
[4] H. Lee, I. K. Kim, T. G. Park, *Bioconjugate Chem.* **2010**, *21*, 289.
[5] J. I. Lee, K. S. Ha, H. S. Yoo, *Acta Biomater.* **2008**, *4*, 791.
[6] J. Jung, A. Solanki, K. A. Memoli, K.-i. Kamei, H. Kim, M. A. Drahl, L. J. Williams, H.-R. Tseng, K. Lee, *Angew. Chem. Int. Ed.* **2010**, *49*, 103.
[7] A. M. Derfus, A. A. Chen, D.-H. Min, E. Ruoslahti, S. N. Bhatia, *Bioconjugate Chem.* **2007**, *18*, 1391.
[8] L. Qi, X. Gao, *ACS Nano* **2008**, *2*, 1403.
[9] M. V. Yezhelyev, L. Qi, R. M. O'Regan, S. Nie, X. Gao, *J. Am. Chem. Soc.* **2008**, *130*, 9006.
[10] M. X. Zhao, J. M. Li, L. Du, C. P. Tan, Q. Xia, Z. W. Mao, L. N. Ji, *Chem. Eur. J.* **2011**, *17*, 5171.
[11] B. Zhang, Y. Zhang, S. K. Mallapragada, A. R. Clapp, *ACS Nano* **2011**, *5*, 129.
[12] D. Siegberg, D.-P. Herten, *Aust. J. Chem.* **2011**, *64*, 512.
[13] T. M. Jovin, *Nat. Biotechnol.* **2003**, *21*, 32.
[14] K. Eisele, R. A. Gropeanu, C. M. Zehendner, A. Rouhanipour, A. Ramanathan, G. Mihov, K. Koynov, C. R. W. Kuhlmann, S. G. Vasudevan, H. J. Luhmann, T. Weil, *Biomaterials* **2010**, *31*, 8789.
[15] W. Bücking, S. Massadeh, A. Merkulov, S. Xu, T. Nann, *Anal. Bioanal. Chem.* **2010**, *396*, 1087.
[16] Q. Wang, Y. Kuo, Y. Wang, G. Shin, C. Ruengruglikit, Q. Huang, *J. Phys. Chem. B* **2006**, *110*, 16860.
[17] Y. Wu, S. Chakrabortty, R. A. Gropeanu, J. Wilhelmi, Y. Xu, K. S. Er, S. L. Kuan, K. Koynov, Y. Chan, T. Weil, *J. Am. Chem. Soc.* **2010**, *132*, 5012.
[18] L. Zöphel, K. Eisele, R. Gropeanu, A. Rouhanipour, K. Koynov, I. Lieberwirth, K. Müllen, T. Weil, *Macromol. Chem. Phys.* **2010**, *211*, 146.
[19] W. R. Algar, U. J. Krull, *ChemPhysChem* **2007**, *8*, 561.
[20] M. H. Stewart, K. Susumu, B. C. Mei, I. L. Medintz, J. B. Delehanty, J. B. Blanco-Canosa, P. E. Dawson, H. Mattoussi, *J. Am. Chem. Soc.* **2010**, *132*, 9804.
[21] J. C. M. van Hest, *Polym. Rev.* **2007**, *47*, 63.
[22] M. A. Dobrovolskaia, P. Aggarwal, J. B. Hall, S. E. McNeil, *Mol. Pharm.* **2008**, *5*, 487.
[23] F. Zhao, Y. Zhao, Y. Liu, X. Chang, C. Chen, *Small* **2011**, *7*, 1322.
[24] S. D. Li, L. Huang, *Gene Ther. 13*, 1313.
[25] J. Liu, X. Yang, K. Wang, R. Yang, H. Ji, L. Yang, C. Wu, *Chem. Commun.* **2011**, *47*, 935.
[26] T. Kim, M. Noh, H. Lee, S.-W. Joo, S. Y. Lee, K. Lee, *J. Phys. Chem. B* **2009**, *113*, 14487.
[27] R. Rigler, E. S. Elson, *Fluorescence Correlation Spectroscopy*, Springer, New York **2001**.
[28] S. A. Kim, K. G. Heinze, P. Schwille, *Nat. Methods* **2007**, *4*, 963.
[29] H. Chen, E. R. Farkas, W. W. Webb, In Vivo Applications of Fluorescence Correlation Spectroscopy, *Methods Cell Biol.* **2008**, *89*, 3–35.
[30] I. A. Khalil, K. Kogure, H. Akita, H. Harashima, *Pharm. Rev.* **2006**, *58*, 32.
[31] O. Boussif, F. Lezoualc'h, M. A. Zanta, M. D. Mergny, D. Scherman, B. Demeneix, J. P. Behr, *Proc. Natl. Acad. Sci. USA* **1995**, *92*, 7297.
[32] P. S. Ghosh, C.-K. Kim, G. Han, N. S. Forbes, V. M. Rotello, *ACS Nano* **2008**, *2*, 2213.
[33] A. J. Lin, N. L. Slack, A. Ahmad, C. X. George, C. E. Samuel, C. R. Safinya, *Biophys. J.* **2003**, *84*, 3307.
[34] M. Howarth, W. Liu, S. Puthenveetil, Y. Zheng, L. F. Marshall, M. M. Schmidt, K. D. Wittrup, M. G. Bawendi, A. Y. Ting, *Nat. Methods* **2008**, *5*, 397.
[35] P. T. Snee, Y. Chan, D. G. Nocera, M. G. Bawendi, *Adv. Mater.* **2005**, *17*, 1131.

Received: February 22, 2012
Revised: June 20, 2012
Published online: August 23, 2012

 © 2012 Wiley-VCH Verlag GmbH & Co. KGaA, Weinheim